Journal of Neuroinflammation

RESEARCH

Open Access

Microglial progranulin differently regulates hypothalamic lysosomal function in lean and obese conditions via cleavage-dependent mechanisms

Chae Beom Park[1†], Chan Hee Lee[2†], Gil Myoung Kang[3], Se Hee Min[4,5] and Min-Seon Kim[4,5*]

Abstract

Progranulin (PGRN) is a secretory precursor protein composed of 7.5 granulins (GRNs). Mutations in the PGRN-encoding gene *Grn* have been associated with neurodegenerative diseases. In our previous study, we found that *Grn* depletion in microglia disrupted glucose metabolism in mice fed a normal chow diet (NCD) but prevented the development of obesity in mice on a high-fat diet (HFD). Given that PGRN regulates lysosomal functions, we investigated lysosomal changes in the hypothalamus of mice with microglia-specific *Grn* depletion. Here we report that microglia-specific *Grn* depletion affects the lysosomes of hypothalamic proopiomelanocortin (POMC) neurons and microglia in diet-dependent fashion. Under NCD conditions, microglial *Grn* depletion led to increased lysosome mass, reduced lysosomal degradative capacity, and accumulation of lipofuscin and cytoplasmic TDP-43 in hypothalamic cells, indicative of lysosomal stress and dysfunction. In contrast, under HFD conditions, the absence of microglial *Grn* suppressed HFD-induced hypothalamic lysosomal stress. In cultured hypothalamic neurons and microglia, PGRN treatment enhanced lysosomal function, an effect inhibited by PGRN cleavage but restored when its cleavage was blocked. Since HFD feeding promotes the cleavage of hypothalamic PGRN into multi-GRNs and GRNs, the diet-dependent lysosomal changes observed in microglial *Grn*-depleted mice may be linked to PGRN cleavage. We also demonstrated that intracerebroventricular injection of bafilomycin, which induces lysosomal stress, resulted in microglial activation, inflammation, disrupted POMC neuronal circuitry, and impaired leptin signaling in the hypothalamus—common features of obesity. Our results indicate that microglial PGRN plays an important role in maintaining hypothalamic lysosomal function under healthy diet conditions, whereas increased cleavage of microglial PGRN in states of overnutrition disrupts hypothalamic lysosomal function, thereby fostering hypothalamic inflammation and obesity.

Keywords Progranulin, Granulin, Hypothalamus, Lysosome, Obesity

[†]Chae Beom Park and Chan Hee Lee contributed equally to this work.

*Correspondence:
Min-Seon Kim
mskim@amc.seoul.kr
[1]Department of Biomedical Science, Asan Medical Institute of Convergence Science and Technology, University of Ulsan College of Medicine, Seoul 05505, Republic of Korea
[2]Department of Biomedical Sciences, Hallym University, Chuncheon 24252, Republic of Korea
[3]Asan Institute for Life Science, Asan Medical Center , Seoul 05505, Republic of Korea
[4]Diabetes Center, Asan Medical Center, Seoul 05505, Republic of Korea
[5]Division of Endocrinology and Metabolism, University of Ulsan College of Medicine, 88 Olympic-ro 43-gil, Songpa-gu, Seoul 05505, Republic of Korea

Introduction

Progranulin (PGRN) is a evolutionarily-conserved secretory precursor protein in mammals of 7.5 granulin (GRN) motifs [1]. PGRN is cleaved to GRNs by proteases such as neutrophil elastase (NE), metalloproteases, proteinase 3, and ADAMTS-7 [2–4], whereas secretory leukocyte peptidase inhibitor (SLPI) inhibits this cleavage [3]. PGRN has numerous regulatory roles in neurobiology, development, wound healing, immune modulation, cancer cell biology, and glucose metabolism [5, 6]. In humans, genetic variations in the PGRN-encoding gene *Grn* are linked to frontotemporal lobar dementia (FTLD), a rare genetic form of this disease [7, 8].

In the central nervous system (CNS), PGRN is produced by neurons and brain-resident immune cell microglia [9]. Studies on humans and mice with *Grn* deficits have offered insights into the roles of microglial PGRN in CNS homeostasis and diseases [10–12]. *Grn*-null mice as well as humans with FTLD-related GRN mutations display abnormal microglia activation in the hippocampus and ventral thalamus [10, 11]. Furthermore, a microglial PGRN deficiency amplifies toxin-induced neuronal injury and loss through an increased production of proinflammatory cytokines [11, 13]. More interestingly, $Grn^{-/-}$ mice show obsessive-compulsive-disorder-like behaviors as a result of a complement-mediated excessive elimination of inhibitory synapses in the ventral thalamus [10]. These prior findings have collectively indicated that PGRN acts to suppress aberrant microglial activation and the complement-mediated removal of synapses.

Lysosomes are critical organelles that break down various biomolecules and other organelles and modulate various cell processes including metabolic and inflammatory signaling pathways [14–16]. The cumulative evidence indicates a strong linkage between PGRN, lysosomes, and neurodegenerative diseases [17, 18]. Humans harboring a homozygous *GRN* mutation develop the lysosomal storage disease known as neuronal ceroid lipofuscinosis [19–21]. FTLD patients that harbor *GRN* mutations also exhibit lysosomal storage material deposition in the brain [20, 21]. These data collectively suggest that a PGRN shortage may lead to lysosomal defects in the brain.

Studies of PGRN using $Grn^{-/-}$ mice have reported conflicting results regarding its regulatory functions. Mice with a generalized or microglial *Grn* deficiency exhibit exaggerated neuroinflammation upon toxic insults or during aging [13, 22] whist $Grn^{-/-}$ mice under high-fat diet (HFD) conditions are metabolically healthier than wild type mice with resistance to HFD-induced obesity and glucose dysregulation due to reduced interleukin-6 production by adipocytes [23]. The mechanisms behind these contrasting outcomes of *Grn* deficiency are still unclear.

The hypothalamus is an important brain region for regulating feeding behavior and whole-body energy homeostasis [24]. This crucial function relies on the ability of hypothalamic neurons, especially those in the arcuate nucleus (ARH), to sense the energy state in peripheral tissues [24]. Accordingly, impeding this ability leads to the development of obesity. Enhanced inflammatory signaling, endoplasmic reticulum stress, mitochondrial dysfunction, and defective autophagy in ARH neurons have been proposed as molecular mechanisms underlying obesity-associated hypothalamic dysfunction [25]. Nevertheless, more mechanisms and contributing factors involved in these pathological processes remain to be elucidated.

Our recent study reported that microglia-released PGRN is involved in maintaining hypothalamic homeostasis and eliciting obesity-related hypothalamic dysfunction [26]. In that study, we showed that ARH microglia produced more PGRN to supply neighboring neurons during chronic consumption of a HFD. Furthermore, microglia-specific *Grn* depletion significantly protected the mice from diet-induced obesity (DIO), with less microglial activation compared to controls. These prior findings from our laboratory suggested that microglia-released *Grn*-derived peptide promotes DIO. In contrast, we further observed that microglia-*Grn* deficient mice exhibited mildly disrupted glucose metabolism and aberrantly activated hypothalamic microglia under normal diet conditions. These diet-dependent differences appear to be linked to increased cleavage of hypothalamic PGRN during obesity progression. Inhibiting PGRN cleavage was shown to attenuate DIO progression, as well as HFD-induced hypothalamic inflammation and microglial activation [26].

Given the aforementioned strong association between PGRN and lysosomal functions [17–21], we decided to investigate lysosomal changes in the hypothalamus of microglia-specific *Grn* deficient mice in the present study. We detected diet-dependent lysosomal changes in the hypothalamus of these mice. We further investigated the mechanisms underlying this phenomenon and the impacts of impaired lysosomal functions on hypothalamic homeostasis and functions.

Materials and methods

Experimental animals

To generate microglia-specific *Grn* deficient mice, $Cx3cr1^{CreER}$:eYFP mice (Jackson Laboratory, #21160) were mated with *Grn*-floxed ($Grn^{f/f}$) mice (Jackson Laboratory, #013174). Gene knockouts were induced through 5 day-intraperitoneal injections of tamoxifen (75 mg/kg/day dissolved in DMSO) at 7 weeks of age. Either $Grn^{f/f}$ or $Cx3cr1^{CreER}$:eYFP littermates were used as wild type controls and all received the same amount of tamoxifen.

C57BL/6 mice at 7–8 weeks of age were purchased from Orient Bio (Seongnam, Korea). All mice had free access to a standard chow diet (Samyang, Seoul, Korea) and water unless indicated otherwise. To generate DIO models, mice were fed an HFD (58% fat; Research Diet, #D12331). Animals were housed under a controlled temperature (22 ± 1°C) and a 12 h light-dark cycle (lights on at 8 AM). All animal procedures were approved by the Institutional Animal Care and Use Committee of the Asan Institute for Life Science (#2012-02-099, July 4, 2012).

Neuron and Microglia Cell Culture

N1 hypothalamic neuronal cells were cultured in DMEM supplemented with 10% fetal bovine serum (FBS) and 1% penicillin/streptomycin (P/S). BV2 microglial cells were maintained in RPMI 1640 media supplemented 10% BSA and 1% P/S.

Immunostaining

Cardiac perfusion was performed in mice with 30 ml saline followed by 30 ml cold 4% paraformaldehyde (PFA) under anesthesia induced with 40 mg/kg Zoletil® and 5 mg/kg Rompun®. Whole brains were collected, post-fixed with 4% PFA at 4 °C for 16 h, and dehydrated in PBS-based 30% sucrose solution until the brain sank to the bottom of the container. Coronal brain slices including the hypothalamus, cortex, and ventral thalamus were sectioned at a 20–30 μm thickness using a cryostat (Leica, Wetzlar, Germany). One out of every five slices was collected and stored at −70 °C.

Hypothalamic slices were blocked with 3% BSA in 0.5% PBST for 1 h at room temperature (RT) unless indicated otherwise. For Tmem119 staining, brain slices were permeabilized with 1% PBST for 5 min at RT and then blocked with 3% BSA dissolved in 1% PBST at RT for 1 h. Subsequently, slices were incubated with primary antibodies at 4 °C for 16 h and then at RT for 1 h with the following dilutions: PGRN (1:100, R&D, #AF2557), Iba1 (1:400, Abcam, #ab5076), CD68 (1:1000, Abcam, #ab53444), Tmem119 (1:500, Abcam, #ab209064), β-endorphin (1:1,000, Phoenix, #H-022-33), C1q (1:1000, Abcam, #ab182451), TFEB (1:500, Bethyl, #A303-673 A), Lamp1 (1:100, BD Pharmingen, #553792), MAP2 (1:1000, Abcam, #ab5392), phospho-STAT3 (P-STAT3; 1:1000, Cell signaling, #9131), and pTDP-43 (1:1000, Protein-Tech, #22309-1AP). After washing, the slides were incubated with the appropriate Alexa-Fluor 488-, 633-, or 647-conjugated secondary antibodies (1:1000) at RT for 1 h. For nuclear staining, slides were counterstained with DAPI (1:10000) for 10 min before mounting. Immunofluorescence was imaged using confocal microscopy (Carl Zeiss 710, Germany). Lipofuscin autofluorescence was observed in brain sections with an emission wavelength of around 500, following PBS washing and DAPI counterstaining. Quantification of fluorescence intensity and cell counting were performed using Image J (NIH, Bethesda, MD) or Photoshop version CS6 (Adobe Systems, San Jose, CA). The fluorescent intensity of approximately 100 cells was analyzed from 3–5 hypothalamic sections per mouse or 5 microscopic fields per well. The number POMC neurons was counted in 3–6 sections per mouse and then multiplied by the total number of hypothalamic slices. Quantitative analysis of the POMC axonal projection intensity in the anterior and posterior hypothalamic paraventricular nucleus (PVH) and dorsomedial nucleus (DMH) areas was conducted as previously described [27].

Lysosomal mass and functions

Lysosomal protein degradation activity was determined using DQ-red BSA (Thermo Fischer Scientific). DQ-BSA and fluorescence-labeled albumin (1:1 mixture, 2 μl) were administered into the dorsal third cerebroventricle using stereotaxic surgery 24 h prior to sacrifice. Brains were collected after 4% PFA cardiac perfusion, post-fixed, and dehydrated in sucrose solution as described in the immunostaining section. For the in vitro experiments, cells were treated with DQ-BSA (10 mg/ml) for 30 min and then washed with PBS three times. Red fluorescence was subsequently observed under confocal microscopy at 0, 1, 2, and 3 h. The DQ-BSA fluorescent intensity in each cell was measured. The data from approximately 100 cells per mouse or per well were presented. Lysosomal mass (total Lamp1 fluorescence intensity) was analyzed with Lamp1 staining. In the in vitro experiments, N1 cells were treated with LysoTracker or LysoSensor probes (Thermo Fischer Scientific; 1:1000) for 30 min at 37 °C prior to fixation. The fluorescent intensity of the LysoTracker or LysoSensor per cell was measured in ~100 cells per well. The enzyme activities of cathepsin B (Immune Chemistry, #937), cathepsin D (Abcam, ab65302), cathepsin L (Immune Chemistry, #941), and v-ATPase (Abcam, ab234055) were assayed in the mediobasal hypothalamus (MBH) using commercial kits in accordance with the manufacturer's protocols.

PGRN cleavage

To induce the cleavage of the PGRN peptide in vitro, the PGRN peptide (500 ng, R&D, #2557-PG-050) was incubated with NE (0.3 units, Sigma, E8140) in a 20 μl buffer (1000 mM Tris-HCl, 960 mM NaCl, pH 8.3) with or without SLPI (500 ng, R&D, #1274-PI-100) at 37°C for 1 h before being applied to cells.

To evaluate PGRN cleavage in the hypothalamus during HFD feeding, protein lysates were extracted from the MBH of mice fed an NCD and mice fed an HFD for 1, 2 and 4 weeks. Immunoblotting was performed using primary antibodies against GRN (1:1000, Atlas,

#HPA008763), PGRN (1:1000, R&D, AF2557), and β-actin (1:1000, Santa Cruz, #sc-47778).

Intracellular PGRN uptake

FITC conjugation of PGRN and NE-processed PGRN fragments (500 ng) was conducted using a commercial kit (Abcam, #ab102884). Briefly, N1 cells were plated in a 12-well plate and cultured in a serum-free medium for 3 h before the uptake study. FITC-conjugated PGRN, PGRN fragments (100 ng each), FITC-PGRN + sortilin inhibitor AF38469 (3 μg, MedchemExpress, #HY12802), and LysoTracker (1:2000) were then applied to the N1 cells on ice for 30 min and allowed to internalize for 5 min at 37 °C. After washing with PBS three times, FITC fluorescence in the lysosomes were measured. Some cells were pretreated with a sortilin inhibitor, AF38469 (3 μg/ml), during the serum-free medium incubation period. In a separate experiment, cells were harvested 5 min post-treatment, and immunoblotting was performed using a PGRN antibody (1:1000, R&D). The intensity of the PGRN band was normalized to that of β-actin.

Quantitative real-time PCR

Hypothalamic tissue blocks were first collected and snap-frozen in liquid nitrogen. Total RNA was then isolated using TRIzol reagent (Thermo Fisher), and cDNA was prepared from the total RNA (2 μg) using M-MLV reverse transcriptase and oligo-dT primers (Invitrogen). The resulting cDNA was amplified on a 7500 Fast Real-Time PCR System (Applied Biosystems). Real-Time PCR was performed in triplicate using SYBR green premix (Enzynomics) using primers (Supplementary Table 1). All quantitative calculations were performed using the $^{\Delta\Delta}$CT method. The mRNA expression levels were normalized to that of glyceraldehyde 3-phosphate dehydrogenase (GAPDH).

In situ hybridization

Mice were perfused with 4% PFA dissolved in DEPC-treated water through the left ventricle. Whole brains were fixed using the same method described in the immunostaining section and then sectioned into 14-μm-thick slices using a cryostat. Fluorescence in situ hybridization (FISH) was performed using RNAscope® fluorescent multiplex reagents provided by Advanced Cell Diagnostics. RNA probes specific to mouse *Grn* (Advanced Cell Diagnostics) were applied to the brain slices, and signal amplification was achieved using multiplex reagents. For double staining of *Grn* and Iba1, the brain slices underwent *Grn* FISH followed by Iba1 immunostaining.

FACS sorting

The hypothalamus was collected from Cx3cr1^{CreER}:eYFP and *Grn*^{MGKO} mice. Cx3cr1:eYFP expressing cells were gated and sorted using fluorescence-activated cell sorting (FACS) with a BD FACS Aria II Cell Sorter. Successful depletion of *Grn* was confirmed through *Grn* qPCR analysis in Cx3cr1:eYFP^{+} and Cx3cr1:eYFP^{-} cells, as previously described [26].

Intracerebroventricular cannulation and injection

Stainless steel cannulas (26 gauge; Plastic One) were implanted into the third ventricle using stereotaxic surgery with the coordinates: 1.4 mm posterior to the bregma, 5.5 mm deep from the sagittal sinus, and 0 mm lateral to the midline. Bafilomycin A1 (MedchemExpress, HY-100558, 50 ng/day dissolved in 1% DMSO-saline) was injected daily into the third ventricle of 8 to 9 week-old C57 mice for 5 days. At the end of the treatments, the mice were sacrificed in the early light phase under freely-fed conditions. Control mice were injected with saline containing the same amount of DMSO. Before sacrifice, leptin (1 μg) was dissolved in 0.9% saline solution and administered via the brain-implanted cannulas. Forty-five minutes after leptin injection, mice were sacrificed to collect the MBH tissues for the assessment of STAT3 signaling. For the SLPI study, SLPI (R&D, #1274-PI-100) was infused into HFD-fed mice via an cerebroventricle-implanted cannula using an Alzet osmotic minipump placed in the subcutaneous tissue of the interscapular area (3 μg/2.6 μl per day for 28 days).

Statistical analysis

All data are presented as mean ± standard error of the mean (SEM). Statistical analyses were performed using SPSS version 24 (IBM Analytics, North Castle, NY) or GraphPad Prism software version 8.0 (GraphPad, San Diego, CA). The sample sizes were selected based on previous studies that used similar methodologies. Statistical significance among the groups was tested using one-way or two-way analysis of variance (ANOVA) followed by a *post-hoc* least significant difference (LSD) test or an unpaired two sided Student's *t*-test if appropriate. All statistical analyses for the animal studies are presented in Supplementary Table 2. Statistical significance was defined at $p < 0.05$.

Results

A microglial PGRN deficiency causes diet-dependent changes in the hypothalamic lysosomes

We confirmed the deletion efficiency of *Grn* in the hypothalamic microglia of *Grn*^{MGKO} mice by performing FACS sorting of hypothalamic microglia followed by *Grn* qPCR analysis or *Grn* in situ hybridization combined with Iba1 double staining in the hypothalamus

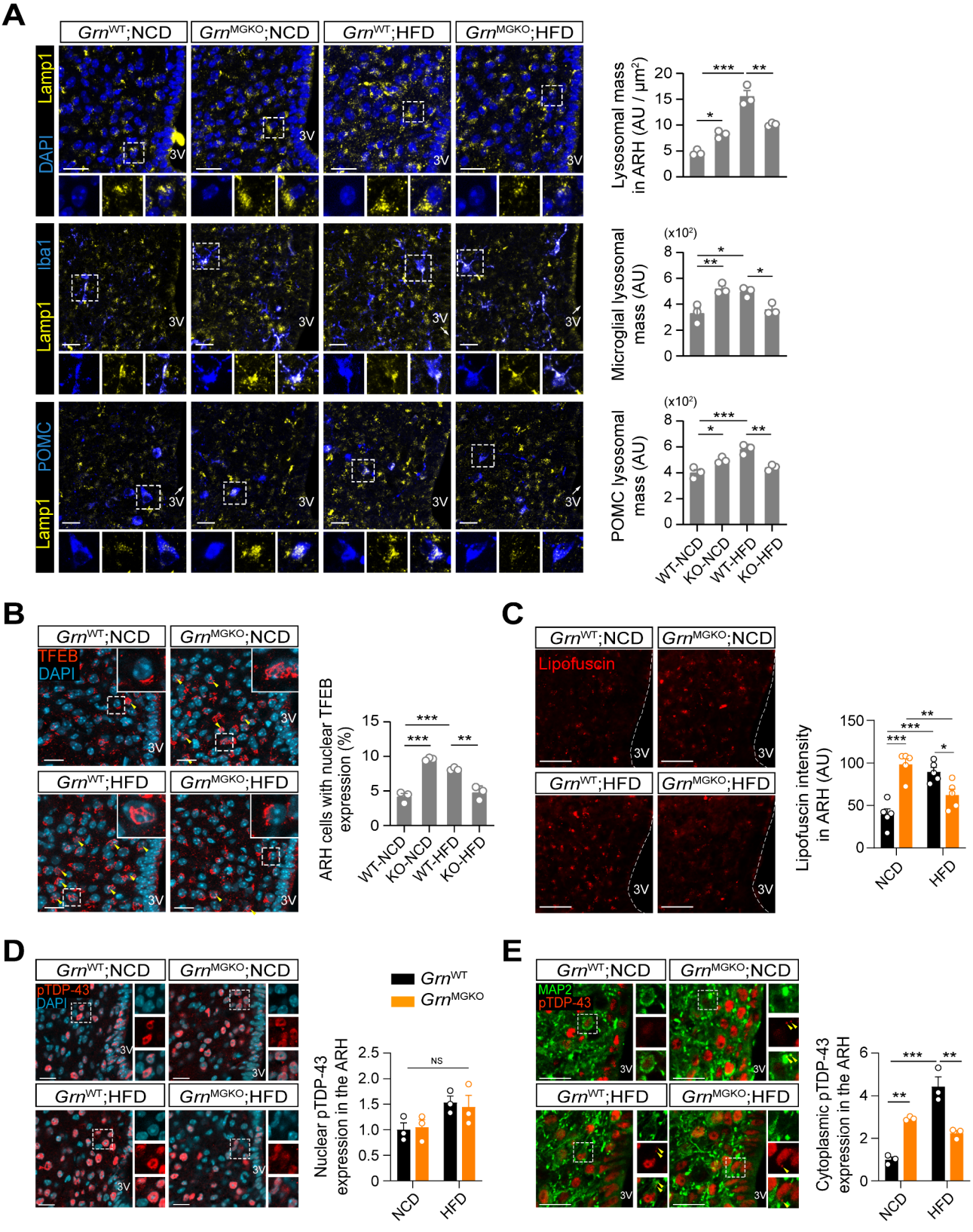

Fig. 1 (See legend on next page.)

(See figure on previous page.)

Fig. 1 Microglial PGRN deficiency induces diet-dependent alterations in hypothalamic lysosomes. (**A**) Representative images and quantification of Lamp1 + lysosome mass in the ARH, specifically in Iba1 + microglia and β-endorphin + POMC neurons of Grn^{WT} and Grn^{MGKO} male mice fed an NCD or HFD for 10 weeks ($n = 3$ mice per group). Approximately 100 cells per mouse were analyzed. Scale bars, 20 µm. (**B**) TFEB immunostaining in the ARH of NCD- or HFD-fed Grn^{WT} mice and Grn^{MGKO} mice ($n = 3$ mice). Scale bars, 20 µm. (**C**) Analysis of lipofuscin expression in the ARH of NCD- or HFD-fed Grn^{WT} mice and Grn^{MGKO} mice ($n = 5$ mice). Scale bars, 50 µm. (**D**, **E**) Double immunostaining of phosphorylated TDP-43 (pTDP-43) and DAPI or MAP2 with quantification of nuclear and cytoplasmic pTDP-43 expression ($n = 3$ mice). Yellow arrowheads indicate cytoplasmic pTDP43 expression. Scale bars, 20 µm
Results are presented as mean ± SEM. *$p < 0.05$, **$p < 0.01$, and ***$p < 0.001$ for indicated group comparisons. NS, not significant

(Supplementary Fig. 1A, B). We then examined lysosomal changes in the ARH of Grn^{MGKO} mice under both NCD- and HFD-fed conditions. We first assessed lysosomal mass using Lamp1 immunostaining and found that under NCD-fed conditions, Grn^{MGKO} male and female mice showed a modest increase in ARH lysosomal mass compared to sex-matched Grn^{WT} mice (Fig. 1A, Supplementary Fig. 2). Upon HFD feeding, Grn^{WT} mice showed a markedly increased lysosomal mass in the ARH compared to NCD-fed conditions. Notably, these lysosomal responses to HFD feeding were obliterated in Grn^{MGKO} mice (Fig. 1A, Supplementary Fig. 2). This pattern of lysosomal changes was observed in the ARH microglia and ß-endorphin^{+} POMC neurons (Fig. 1A). As CD68 is a marker for microglia-specific lysosomes [28], we also performed CD68 immunostaining. The results revealed similar lysosomal changes in ARH microglia of Grn^{MGKO} male mice (Supplementary Fig. 3). Hence, the microglia-specific deletion of *Grn* caused diet-dependent opposite lysosomal mass in ARH neurons and microglia.

A previous study has reported that CD68 expression remained unchanged in the cortex and thalamus of 10-week-old $Grn^{-/-}$ mice [29]. We thus investigated lysosomal changes in other brain regions of 17-week-old Grn^{MGKO} mice fed a NCD. Consistent with a previous report [29], CD68 immunostaining showed no significant lysosomal alterations in the cortex or ventral thalamus (Supplementary Fig. 4). These findings suggest that microglial *Grn* deficiency induces lysosomal changes in a brain region-specific manner, at least in young mice.

Transcription factor EB (TFEB) is a master regulator of lysosomal biogenesis [30]. Once activated, TFEB shuttles to the nucleus and initiates the transcription of lysosomal genes [30]. We thus investigated TFEB activation in the ARH of our mouse models by measuring its nuclear expression. In line with the observed lysosomal changes (Fig. 1A), the numbers of ARH cells with nuclear TFEB expression were significantly higher in Grn^{MGKO} mice than in Grn^{WT} mice that had been NCD fed (Fig. 1B). TFEB activation was induced by HFD feeding in Grn^{WT} mice, but these responses were blunted in Grn^{MGKO} mice (Fig. 1B). These data suggest that TFEB may mediate the changes in the lysosomal mass that are induced by a *Grn* deficiency and HFD feeding.

We also assessed hypothalamic lysosomal functions with lipofuscin expression, a pigmented byproduct of lysosomal degradation, and its accumulation implying lysosomal dysfunction [31]. We found a significant increase in lipofuscin accumulation in the ARH of Grn^{MGKO} mice compared with the Grn^{WT} mice under NCD conditions (Fig. 1C). Grn^{WT} mice had increased lipofuscin expression in their ARH when exposed to HFD consumption and this change become insignificant in Grn^{MGKO} mice (Fig. 1C). TDP-43 is a nuclear RNA-binding protein whose accumulation in the cytoplasm is associated with impaired lysosomal clearance and observed in neurodegenerative diseases such as amyotrophic lateral sclerosis, Alzheimer's disease, and FTLD [32, 33]. Immunostaining using phosphorylated TDP-43 (pTDP-43) antibody in the hypothalamus revealed that nuclear pTDP-43 expression, assessed by the colocalization of pTDP43 and DAPI, remained unchanged in our mouse models under diet manipulation (Fig. 1D). In contrast, the cytoplasmic expression of pTDP-43, evaluated by the colocalization of pTDP43 and the neuronal cytoplasmic marker MAP2, exhibited changes similar to those observed in lipofuscin expression (Fig. 1E). These data collectively indicated that opposing lysosomal changes occurred in the hypothalamus of microglial *Grn*-deficient mice depending on whether the animals were given an NCD or HFD. In contrast to the hypothalamus, both nuclear and cytoplasmic pTDP-43 expression in the cortex and ventral thalamus of young Grn^{MGKO} mice was barely detectable and showed no significant differences compared to Grn^{WT} mice (Supplementary Fig. 5). We further assessed lysosomal protein degradation capacity with DQ-BSA, which produces red fluorescent products upon hydrolysis by lysosomal proteases [27]. Fluorescence-labeled albumin (Fl-albumin) was co-injected to monitor the success of the injection and the cellular uptake of DQ-BSA, which might influence DQ-BSA signals. In Grn^{WT} mice, HFD consumption significantly reduced the DQ-BSA signal in ARH POMC neurons and microglia, with no significant alteration in Fl-albumin signals (Fig. 2A, B, and Supplementary Fig. 6). This result indicates that chronic HFD consumption impairs lysosomal protein degradation capacity in the hypothalamic neurons and microglia despite an increased lysosomal mass. On the other hand, ARH microglia and neurons of Grn^{MGKO} mice had lower DQ-BSA signals under NCD-fed conditions but higher DQ-BSA signals in HFD-fed conditions (Fig. 2A, B).

We further measured lysosomal protease activities in the MBH. Grn^{WT} mice had decreased hypothalamic

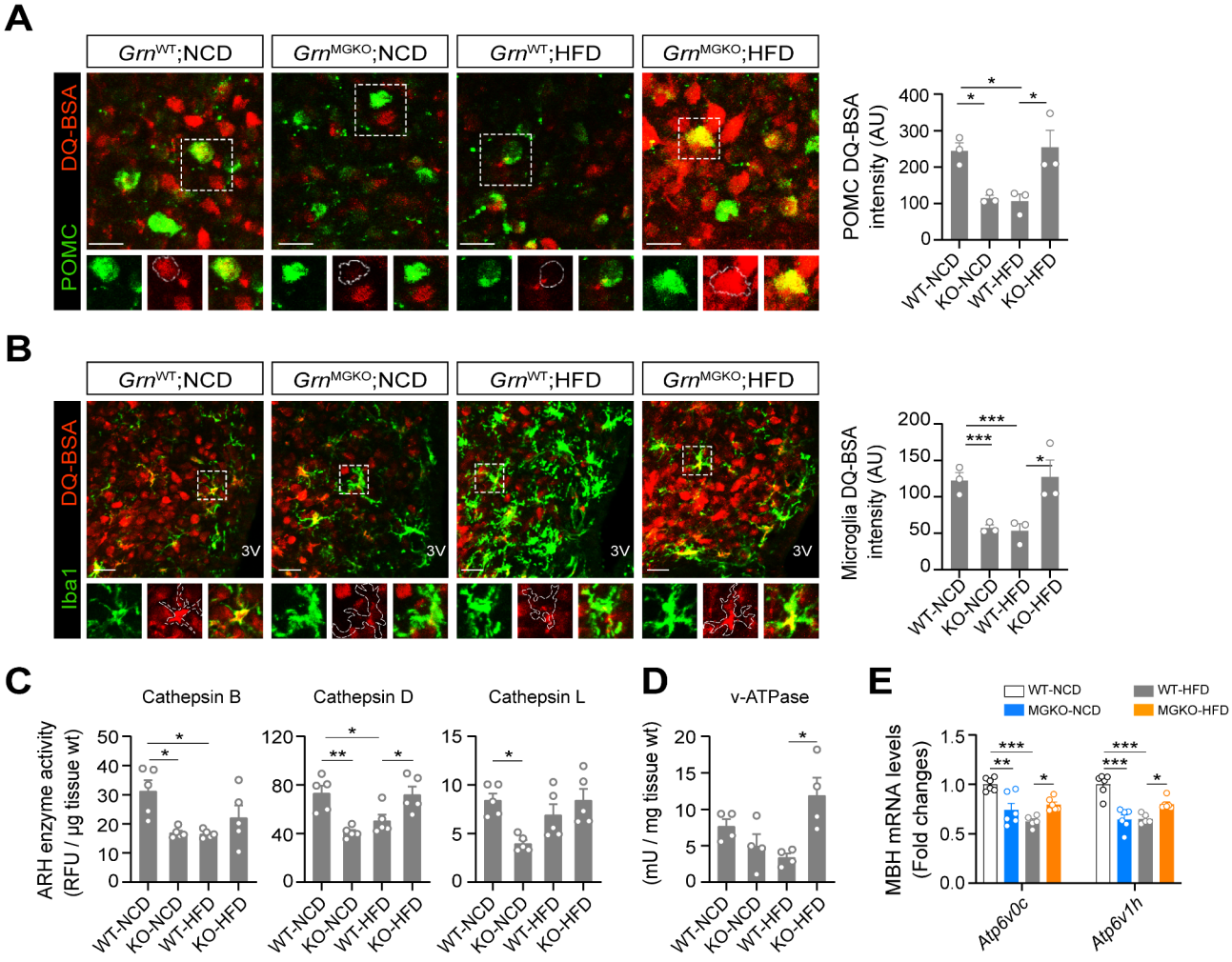

Fig. 2 Altered lysosomal proteolysis in the hypothalamus of mice harboring a microglial *Grn* depletion. (**A**, **B**) Representative images and measurement of DQ-BSA in the ARH POMC neurons and Iba1$^+$ microglia of NCD- of HFD-fed *Grn*^{WT} and *Grn*^{MGKO} male mice. ($n = 3$ mice). About 100 cells per mouse were analyzed. Scale bars, 20 μm. (**C**, **D**) Hypothalamic lysosomal cathepsin B, D, and L activities and v-ATPase activity in *Grn*^{WT} and *Grn*^{MGKO} male mice fed on an NCD or HFD ($n = 5$). (**E**) qPCR analysis of mRNA expression of v-ATPase subunits *Atp6v0c* and *Atp6v1h* in the MBH of *Grn*^{WT} and *Grn*^{MGKO} males fed on an NCD or HFD ($n = 5$–6)

Results are presented as a mean value ± SEM. *$p < 0.05$, **$p < 0.01$, and ***$p < 0.001$ between indicated groups. NS, not significant

cathepsin B and D (CTSB, CTSD) activities upon HFD feeding (Fig. 2C). *Grn*^{MGKO} mice showed lower CTSB, CTSD, and CTSL activities in the NCD-fed condition but higher CTSD activity with HFD feeding (Fig. 2C), which was consistent with the DQ-BSA data (Fig. 2A, B). These findings implied that microglia-derived *Grn* products may control hypothalamic lysosomal degradative functions in a diet-dependent manner. It was notable that this regulation occurs in both a cell-autonomous (microglia) and non-autonomous (neurons) fashion.

The intraluminal pH of lysosomes, crucial for optimal lysosomal enzyme activity, is maintained within an acidic range (pH 4.5–5) by the vacuolar ATPase (v-ATPase) proton pump [34]. Measurements of v-ATPase activity indicated that HFD feeding tended to reduce v-ATPase activity in the MBH of *Grn*^{WT} mice. However, *Grn*^{MGKO} HFD mice exhibited higher v-ATPase activity compared to their diet-matched controls (Fig. 2D). Similarly, chronic HFD feeding decreased the mRNA expression of hypothalamic v-ATPase subunits (Fig. 2E). Specifically, *Atp6v0c* and *Atp6v1h* mRNA expression levels were decreased in *Grn*^{MGKO} NCD mice and increased in *Grn*^{MGKO} HFD mice compared to *Grn*^{WT} mice on the same diet (Fig. 2E). These findings suggest that microglia-released *Grn*-derived peptides modulate hypothalamic lysosomal functions, at least in part, through the regulation of v-ATPase activity and, consequently, lysosomal pH.

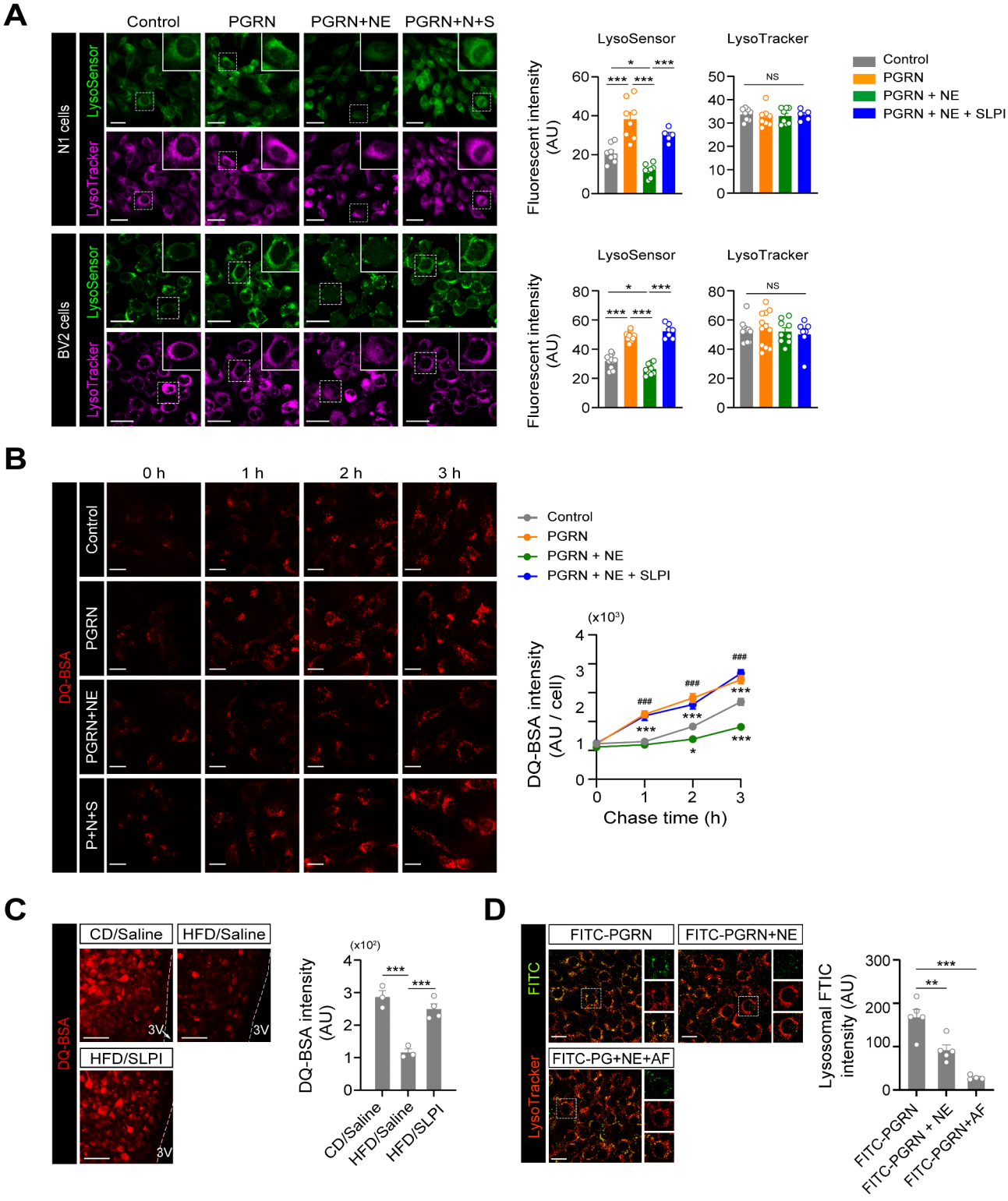

Fig. 3 (See legend on next page.)

Extracellular cleavage inhibits PGRN regulation of lysosomal functions in hypothalamic neurons and microglia

We further investigated the mechanism underlying the opposite lysosomal changes in Grn^{MGKO} mice under NCD and HFD conditions. The cleavage of PGRN into multi-GRNs and GRNs was enhanced in the hypothalamus under HFD conditions (Supplementary Fig. 7). Thus,

(See figure on previous page.)

Fig. 3 Extracellular cleavage impairs PGRN-mediated regulation of lysosomal functions in hypothalamic neurons and microglia. (**A**) Effects of treatment with PGRN alone, PGRN + NE, or PGRN + NE + SLPI on lysosomal pH (LysoSensor) and lysosomal mass (LysoTracker) in N1 hypothalamic neurons and BV2 microglia cells over a 3-h period. Approximately 100 cells were analyzed per group ($n = 5–12$ wells). Scale bars, 20 µm. (**B**) DQ-BSA pulse-chase assay in N1 cells treated with PGRN alone, PGRN + NE, or PGRN + NE + SLPI. Approximately 100 cells were analyzed per group ($n = 5–8$ wells). Scale bars, 25 µm. (**C**) Representative images and quantification of DQ-BSA signals in the ARH of mice fed an NCD or HFD for 10 weeks and treated with SLPI for 4 weeks prior to sacrifice. Approximately 100 cells per mouse were analyzed ($n = 3–4$). Scale bars, 20 µm. (**D**) Cellular uptake and lysosomal localization of FITC-labeled PGRN and FITC-labeled PGRN fragments ($n = 100$ cells). To induce PGRN cleavage, FITC-labeled PGRN was pre-incubated with NE for 1 h before treatment. Peptides were then allowed to traffic to lysosomes in N1 hypothalamic neuron cells for 1 h before fixation. The sortilin inhibitor AF38469 was used to confirm the sortilin-dependence of PGRN uptake ($n = 4–5$ wells). Scale bars, 20 µm. Results are presented as mean ± SEM. $^{*}p < 0.05$, $^{**}p < 0.01$, and $^{***}p < 0.001$ for comparisons between indicated groups or controls at each time point. $^{\#\#\#}p < 0.005$ vs. PGRN + NE at each time point. NS, not significant

we tested whether the extracellular cleavage of PGRN affected its regulation of lysosomal functions in hypothalamic neurons and microglia. In this study, we assessed lysosomal mass with the LysoTracker probe and lysosomal pH with the LysoSensor probe in N1 hypothalamic neuronal cells and BV2 microglia cells. PGRN cleavage was induced by cotreatment of PGRN and NE for 1 h at 37 °C before cell treatment, and inhibition of PGRN cleavage was achieved by adding SLPI to the PGRN and NE mixture. We confirmed PGRN degradation to 25 kDa and 15 kDa fragments (multi-GRNs), and its inhibition with SLPI, by western blotting before performing subsequent experiments (Supplementary Fig. 8).

Treatment with PGRN alone increased LysoSensor signal levels, while treatment with PGRN cleavage products did not produce this effect and instead mildly decreased LysoSensor signal levels in both N1 hypothalamic neuronal cells and BV2 microglial cells (Fig. 3A). Notably, inhibition of PGRN cleavage with SLPI restored PGRN-induced lysosomal acidification (Fig. 3A). In contrast, LysoTracker signals showed no significant changes under any of these treatment conditions (Fig. 3A). These findings suggest that acute PGRN treatment promotes lysosomal acidification in hypothalamic neurons and microglia. However, once cleaved extracellularly, PGRN loses this capacity, and its cleavage products may impair lysosomal acidification.

We further investigated the effects of PGRN and its cleavage on lysosomal proteolytic capacity using a DQ-BSA pulse-chase assay. N1 cells were incubated with DQ-BSA for 30 min (pulse), washed, and then observed for 3 h (chase) to monitor the red fluorescence intensity generated by DQ-BSA hydrolysis by lysosomal proteases. PGRN treatment enhanced the increase in DQ-BSA signal intensity whereas treatment with PGRN-cleaved products inhibited it (Fig. 3B). Moreover, co-treatment with SLPI fully restored the effect of PGRN on DQ-BSA hydrolysis (Fig. 3B). Consistent with these in vitro findings, SLPI treatment, which blocks NE-induced PGRN proteolysis, improved the HFD-induced reduction in hypothalamic DQ-BSA signal in mice (Fig. 3C). These results support the possibility that NE-induced extracellular PGRN degradation contributes to lysosomal dysfunction in the hypothalamus of DIO mice.

Extracellular PGRN is incorporated into cells via a sortilin-mediated mechanisms [35]. Following endocytosis, PGRN is transported to lysosomes, where it controls their acidification and hydrolysis [18]. As endocytosis may be the first step in the regulation of lysosomal function by extracellular PGRN, we examined whether extracellular cleavage may impair cellular uptake of PGRN by monitoring the cellular uptake of FITC-labeled PGRN in N1 cells. Cellular uptake and lysosomal localization of FITC-PGRN signals were profoundly decreased by cotreatment of the cells with the sortilin inhibitor AF38469 (Fig. 3D), suggesting that endocytosis of FITC-PGRN is dependent on sortilin. Likewise, cotreatment of the cells with FITC-PGRN and NE diminished the lysosomal localization of FITC-PGRN (Fig. 3D). PGRN immunoblotting in cell lysates revealed that treatment with cleaved FITC-PGRN induced a smaller increase in intracellular PGRN and multi-GRN expression levels compared to treatment with FITC-PGRN alone (Supplementary Fig. 9). These results suggest that the reduced FITC signals in lysosomes may not result from proteolysis of FITC-PGRN within the lysosomes. Instead, extracellular proteolysis of PGRN may impair its cellular uptake and lysosomal trafficking.

Hypothalamic lysosomal dysfunction leads to hypothalamic microglia activation, inflammation, and defects in POMC neuron functions and circuits

To investigate whether impaired lysosomal function itself contributes to obesity-related hypothalamic pathologies, we induced hypothalamic lysosomal dysfunction by administering a low dose of bafilomycin-A1, a compound that disrupts lysosomal acidification [36], into the cerebroventricle of NCD-fed C57 mice for five days. This treatment successfully induced lysosomal dysfunction in the ARH, as evidenced by increased lysosomal mass and reduced DQ-BSA signals, particularly in POMC neurons (Fig. 4A, B). Short-term bafilomycin treatment triggered reactive microgliosis, demonstrated by a reduction in $Tmem119^{+}$ microglia and an increase in $Iba1^{+}$ microglia, along with elevated expression of the microglial complement protein C1q in NCD-fed mice (Fig. 4C, D). These findings indicate that bafilomycin-induced lysosomal stress activates hypothalamic microglia and drives their overproduction of complement.

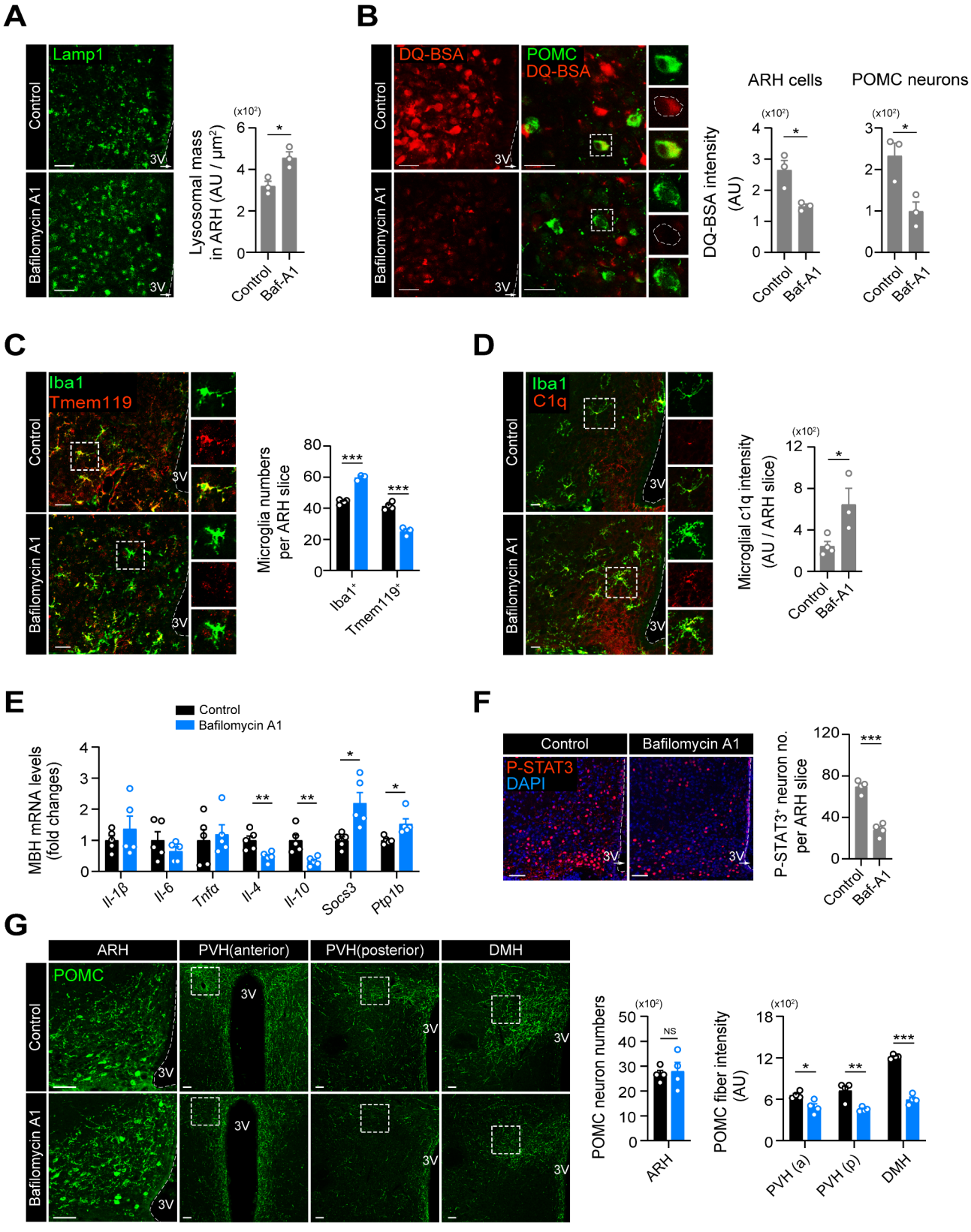

Fig. 4 (See legend on next page.)

(See figure on previous page.)

Fig. 4 Hypothalamic lysosomal dysfunction leads to hypothalamic microglia activation, inflammation, and defects in POMC neuron functions and circuits. (**A**, **B**) Induction of hypothalamic lysosomal stress via an ICV injection of bafilomycin, measured by an increased lysosomal mass (Lamp1) and reduced DQ-BSA signals and in the ARH, especially in POMC neurons ($n=3$). About 100 cells per mouse were analyzed ($n=3$). Scale bars, 20 µm. (**C**, **D**) Hypothalamic microglia activation and C1q overproduction in male mice injected with ICV bafilomycin. About 100 cells per mouse were analyzed ($n=3$–4). Scale bars, 20 µm. (**E**) qPCR analysis of hypothalamic proinflammatory and anti-inflammatory cytokine expression and leptin signaling inhibitors in saline- or bafilomycin-injected mice ($n=5$). (**F**) Reduced leptin-induced P-STAT3 expression in the ARH of bafilomycin-injected mice ($n=4$). Scale bars, 50 µm. (**G**) Reduced POMC axonal density in the anterior and posterior regions of the PVH and DMH, with no changes in POMC neuron numbers in the hypothalamic ARH ($n=4$). Scale bars, 50 µm

Results are presented as a mean value ± SEM. *$p<0.05$, **$p<0.01$, and ***$p<0.001$ between indicated groups. NS, not significant

Moreover, bafilomycin treatment reduced the expression of anti-inflammatory cytokines (*Il-4* and *Il-10*) in the MBH without inducing significant changes in proinflammatory cytokine expression (Fig. 4E). Given the balance between proinflammatory and anti-inflammatory regulators, these changes would favor hypothalamic inflammation. Bafilomycin treatment also increased the hypothalamic expression of *Socs3* and *Ptp1b* (Fig. 4E), both of which are known to inhibit the signaling pathway of the critical anti-obesity hormone leptin in hypothalamic neurons [37]. We therefore investigated hypothalamic leptin signaling in bafilomycin-injected mice. ICV leptin-induced STAT3 phosphorylation was markedly decreased in the ARH of mice receiving bafilomycin compared to control animals injected with saline (Fig. 4F), although short-term treatment of bafilomycin did not increase body weight (data not shown). Consistently, when assessing hypothalamic leptin signaling in Grn^{MGKO} NCD mice and Grn^{MGKO} HFD mice, Grn^{MGKO} NCD mice with impaired hypothalamic lysosomal function exhibited a reduced phospho-STAT3 response to leptin, compared to Grn^{WT} NCD mice (Supplementary Fig. 10). In contrast, Grn^{MGKO} HFD mice with improved lysosomal function showed enhanced leptin signaling compared to Grn^{WT} HFD mice (Supplementary Fig. 10).

Finally, we evaluated whether bafilomycin treatment affects the number of POMC neurons and their axonal projections. While ARH POMC neuron numbers remained unchanged, bafilomycin-injected mice showed a marked reduction in POMC axonal density in PVH and DMH (Fig. 4G). These findings suggest that hypothalamic lysosomal dysfunction, potentially driven by microglial PGRN cleavage, may contribute to hypothalamic microglial activation, inflammation, ARH neuronal insensitivity to leptin, and disruption of POMC neuronal circuits in the context of overnutrition, thereby promoting the development of obesity and metabolic disorders.

Discussion

In this study, microglial *Grn* deficiency in mice led to lysosomal alterations in the hypothalamic ARH. Specifically, NCD-fed Grn^{MGKO} mice showed increased lysosomal mass, reduced lysosomal degradative capacity and protease activity, and an accumulation of lipofuscin and cytoplasmic pTDP-43 in the hypothalamus, all indicative of lysosomal dysfunction. However, under HFD-fed conditions, these mice exhibited improved lysosomal function. In vitro, PGRN treatment enhanced lysosomal acidification and protein degradation capacity in hypothalamic neurons and microglia, whereas PGRN cleavage products lacked these effects on lysosomes. Additionally, SLPI treatment, which inhibits PGRN cleavage, improved hypothalamic lysosomal function in HFD-fed obese mice, suggesting that PGRN cleavage negatively impacts hypothalamic lysosomal function in conditions of obesity. These findings underscore cleavage-dependent regulatory roles of PGRN in hypothalamic lysosomal function.

Notably, unlike the changes observed in the hypothalamus, microglial *Grn* deficiency did not induce lysosomal alterations in the cortex or ventral thalamus during the young adult period under NCD-fed conditions. These findings are consistent with a previous study reporting no lysosomal changes in these brain regions in 10-week-old $Grn^{-/-}$ mice, although these mice exhibited increased lysosomal dysfunction when analyzed at 90 weeks of age [29]. Furthermore, $Grn^{-/-}$ mice display an age-dependent increase in TDP-43 pathology, with no significant changes observed until 12 months of age [38]. These findings align with our observation that NCD-fed Grn^{MGKO} young mice did not show TDP-43 pathology in the cortex or thalamus. Collectively, these results suggest that microglial *Grn* deficiency induces lysosomal changes specifically in the hypothalamus of young-aged mice. The factors contributing to these hypothalamus-specific lysosomal changes in young Grn^{MGKO} mice remain unclear. One possible explanation is that dietary components, such as fatty acids, may more easily access the hypothalamus and influence lysosomal function in a manner dependent on the presence or absence of microglial PGRN.

So far, several mechanisms via which PGRN controls lysosomal functions have been proposed. One suggestion is that PGRN directly binds to CTSD which promotes CTSD maturation, thereby controlling lysosomal proteolysis [39, 40]. In our study, a microglial *Grn* deficiency altered hypothalamic CTSD activity in a diet-dependent manner. A second hypothesis is that PGRN facilitates the lysosomal acidification process, which may impact global lysosomal hydrolysis. In supporting of this possibility, we found that treatment of PGRN and its cleaved products,

significantly altered the lysosomal pH in the mouse hypothalamic neurons and microglia cells. As Grn^{MGKO} mice exhibited altered v-ATPase activity and expression in the MBH, we speculate that PGRN may regulate lysosomal pH through the regulation of v-APTase. A third mechanistic proposal is that PGRN regulates glucocerebrosidase (GCase) activity [41–43] and a fourth is that it regulates lysosomal lipid hydrolysis by maintaining endolysosomal phospholipid bis(monoacylglycero) phosphate (BMP) levels [44, 45]. Another suggested mechanism is that PGRN controls the endolysosomal trafficking of lysosomal proteins [46].

Regarding the potential mechanism underlying the adverse effects of extracellular PGRN cleavage on lysosomes, impaired lysosomal trafficking of PGRN cleavage products is a likely explanation. Our findings show that NE-induced PGRN cleavage reduces the cellular uptake and lysosomal localization of fluorescence-labeled PGRN. Moreover, the intracellular PGRN content was significantly lower in hypothalamic neuronal cells treated with cleaved PGRN compared to those treated with full-length PGRN. Since sortilin and PSAP mediate the endocytosis and lysosomal trafficking of PGRN through interactions with its C-terminus [47, 48], PGRN cleavage products lacking these interaction sites may fail to effectively reach lysosomes. Additionally, PGRN cleavage may produce GRNs with harmful effects on lysosomes. The finding that microglial *Grn* deficiency alleviates HFD-induced lysosomal stress and dysfunction suggests a detrimental role for certain *Grn*-derived peptides on lysosomes. Consistently, in *C. elegans*, GRN overexpression in the absence of PGRN impairs lysosomal degradation and exacerbates TDP43 neurotoxicity [49]. This hypothesis could be further tested if individual GRN peptides become commercially available. Our study establishes a causal link between lysosomal dysfunction in ARH neurons and the development of metabolic dysregulation or obesity. Inducing hypothalamic lysosomal dysfunction in mice through bafilomycin injections resulted in hypothalamic microglial activation and impaired leptin signaling in ARH neurons—key features commonly observed in diet-induced obesity [50]. Further investigation is needed to determine whether long-term ICV bafilomycin treatment could induce obesity or metabolic impairments. In addition, our current study and previous study [26] demonstrate that NCD-fed Grn^{MGKO} mice exhibit hypothalamic lysosomal dysfunction, fasting hyperglycemia, hypothalamic microglial activation, and impaired leptin signaling, despite no changes in adiposity. In contrast, HFD-fed Grn^{MGKO} mice show significant improvement in HFD-induced hypothalamic lysosomal dysfunction. These mice are resistant to the development of HFD-induced obesity and metabolic dysregulation, accompanied by reduced hypothalamic inflammation and improved leptin signaling. These findings suggest that hypothalamic lysosomal dysfunction may drive metabolic disorders or obesity through microglia-mediated inflammatory responses and disrupted hypothalamic sensing of peripheral metabolic signals, such as leptin, which are key contributors to the development and progression of obesity and its metabolic complications [37, 50]. Furthermore, microglia with lysosomal dysfunction may exacerbate metabolic disorders or obesity by impairing synaptic pruning of hypothalamic neurons, as evidenced by the upregulation of complement C1q expression in the ARH following bafilomycin treatment. Lysosomal defects in hypothalamic neurons may also disrupt axonal homeostasis by impairing the axonal transport of endolysosomes [44], thereby compromising the integrity of the POMC neuronal circuit, which is critical for maintaining energy balance and euglycemia.

In our study, we induced the depletion of microglial *Grn* in young adult mice. To better understand the importance of microglial *Grn* in the context of aging-related neurodegenerative disorders, it may be necessary to induce microglial *Grn* depletion in aged mice. Furthermore, considering the brain region-specific effects of microglial *Grn* deficiency on lysosomes, a mouse model with brain region-specific microglial *Grn* depletion may be required to elucidate the role of *Grn* in microglia within specific brain regions.

In summary, our study highlights the importance of microglia-released PGRN for normal hypothalamic lysosomal function and whole-body metabolic homeostasis. Our findings also reveal the potential risk of extracellular PGRN cleavage and its detrimental impact on hypothalamic lysosomal function under conditions of overnutrition. Diet-dependent processing of PGRN and its biological consequences provide another layer of complexity in PGRN biology that needs to be considered if designing therapeutic strategies aimed at increasing brain PGRN levels to treat neurodegenerative diseases.

Supplementary Information

The online version contains supplementary material available at https://doi.org/10.1186/s12974-025-03370-1.

Supplementary Material 1

Supplementary Material 2

Acknowledgements

This study was supported by grants from the National Research Foundation of Korea (NRF), funded by the Ministry of Science and ICT of Korea (2020R1A2C3004843, 2022M3E5E8017213, 2022R1C1C1004187), and by the Korea Health Technology R&D Project through the Korea Health Industry Development Institute (KHIDI), funded by the Ministry of Health & Welfare, Republic of Korea (RS-2024-00438349, RS-2024-00404132).

Author contributions

C.B.P., C.H.L., and M.-S.K. designed the study. C.B.P., C.H.L., and G.M.K. performed the experiments and/or analyzed the data. S.H.K discussed the data. C.B.P.,

C.H.L., and M.-S.K. wrote the manuscript. All authors read and edited the manuscript and approved the final version.

Data availability
No datasets were generated or analysed during the current study.

Declarations

Ethics declaration
Not applicable.

Competing interests
The authors declare no competing interests.

Received: 11 November 2024 / Accepted: 6 February 2025
Published online: 07 March 2025

References

1. Palfree RG, Bennett HP, Bateman A. The evolution of the Secreted Regulatory protein progranulin. PLoS ONE. 2015;10:e0133749.
2. Kessenbrock K, Fröhlich L, Sixt M, Lämmermann T, Pfister H, Bateman A, Belaaouaj A, Ring J, Ollert M, Fässler R, Jenne DE. Proteinase 3 and neutrophil elastase enhance inflammation in mice by inactivating antiinflammatory progranulin. J Clin Invest. 2008;118:2438–47.
3. Zhu J, Nathan C, Jin W, Sim D, Ashcroft GS, Wahl SM, Lacomis L, Erdjument-Bromage H, Tempst P, Wright CD, Ding A. Conversion of proepithelin to epithelins: roles of SLPI and elastase in host defense and wound repair. Cell. 2002;111:867–78.
4. Bai XH, Wang DW, Kong L, Zhang Y, Luan Y, Kobayashi T, Kronenberg HM, Yu XP, Liu CJ. ADAMTS-7, a direct target of PTHrP, adversely regulates endochondral bone growth by associating with and inactivating GEP growth factor. Mol Cell Biol. 2009;29:4201–19.
5. Toh H, Chitramuthu BP, Bennett HP, Bateman A. Structure, function, and mechanism of progranulin; the brain and beyond. J Mol Neurosci. 2011;45:538–48.
6. Cenik B, Sephton CF, Kutluk Cenik B, Herz J, Yu G. Progranulin: a Proteolytically Processed protein at the crossroads of inflammation and Neurodegeneration*. J Biol Chem. 2012;287:32298–306.
7. Cruts M, Gijselinck I, van der Zee J, Engelborghs S, Wils H, Pirici D, Rademakers R, Vandenberghe R, Dermaut B, Martin JJ, et al. Null mutations in progranulin cause ubiquitin-positive frontotemporal dementia linked to chromosome 17q21. Nature. 2006;442:920–4.
8. Baker M, Mackenzie IR, Pickering-Brown SM, Gass J, Rademakers R, Lindholm C, Snowden J, Adamson J, Sadovnick AD, Rollinson S, et al. Mutations in progranulin cause tau-negative frontotemporal dementia linked to chromosome 17. Nature. 2006;442:916–9.
9. Petkau TL, Neal SJ, Orban PC, MacDonald JL, Hill AM, Lu G, Feldman HH, Mackenzie IR, Leavitt BR. Progranulin expression in the developing and adult murine brain. J Comp Neurol. 2010;518:3931–47.
10. Lui H, Zhang J, Makinson Stefanie R, Cahill Michelle K, Kelley Kevin W, Huang H-Y, Shang Y, Oldham Michael C, Martens Lauren H, Gao F, et al. Progranulin Deficiency Promotes Circuit-specific synaptic pruning by Microglia via complement activation. Cell. 2016;165:921–35.
11. Yin F, Banerjee R, Thomas B, Zhou P, Qian L, Jia T, Ma X, Ma Y, Iadecola C, Beal MF, et al. Exaggerated inflammation, impaired host defense, and neuropathology in progranulin-deficient mice. J Exp Med. 2010;207:117–28.
12. Sakae N, Roemer SF, Bieniek KF, Murray ME, Baker MC, Kasanuki K, Graff-Radford NR, Petrucelli L, Van Blitterswijk M, Rademakers R, Dickson DW. Microglia in frontotemporal lobar degeneration with progranulin or C9ORF72 mutations. Ann Clin Transl Neurol. 2019;6:1782–96.
13. Martens LH, Zhang J, Barmada SJ, Zhou P, Kamiya S, Sun B, Min SW, Gan L, Finkbeiner S, Huang EJ, Farese RV Jr. Progranulin deficiency promotes neuroinflammation and neuron loss following toxin-induced injury. J Clin Invest. 2012;122:3955–9.
14. Perera RM, Zoncu R. The lysosome as a Regulatory Hub. Annu Rev Cell Dev Biol. 2016;32:223–53.
15. Settembre C, Fraldi A, Medina DL, Ballabio A. Signals from the lysosome: a control centre for cellular clearance and energy metabolism. Nat Rev Mol Cell Biol. 2013;14:283–96.
16. Ge W, Li D, Gao Y, Cao X. The roles of lysosomes in inflammation and Autoimmune diseases. Int Rev Immunol. 2015;34:415–31.
17. Kao AW, McKay A, Singh PP, Brunet A, Huang EJ. Progranulin, lysosomal regulation and neurodegenerative disease. Nat Rev Neurosci. 2017;18:325–33.
18. Paushter DH, Du H, Feng T, Hu F. The lysosomal function of progranulin, a guardian against neurodegeneration. Acta Neuropathol. 2018;136:1–17.
19. Almeida MR, Macário MC, Ramos L, Baldeiras I, Ribeiro MH, Santana I. Portuguese family with the co-occurrence of frontotemporal lobar degeneration and neuronal ceroid lipofuscinosis phenotypes due to progranulin gene mutation. *Neurobiology of Aging* 2016, 41:200.e201-200.e205.
20. Smith KR, Damiano J, Franceschetti S, Carpenter S, Canafoglia L, Morbin M, Rossi G, Pareyson D, Mole SE, Staropoli JF, et al. Strikingly different clinicopathological phenotypes determined by progranulin-mutation dosage. Am J Hum Genet. 2012;90:1102–7.
21. Ward ME, Chen R, Huang HY, Ludwig C, Telpoukhovskaia M, Taubes A, Boudin H, Minami SS, Reichert M, Albrecht P et al. Individuals with progranulin haploinsufficiency exhibit features of neuronal ceroid lipofuscinosis. Sci Transl Med 2017, 9.
22. Yin F, Dumont M, Banerjee R, Ma Y, Li H, Lin MT, Beal MF, Nathan C, Thomas B, Ding A. Behavioral deficits and progressive neuropathology in progranulin-deficient mice: a mouse model of frontotemporal dementia. Faseb j. 2010;24:4639–47.
23. Matsubara T, Mita A, Minami K, Hosooka T, Kitazawa S, Takahashi K, Tamori Y, Yokoi N, Watanabe M, Matsuo E, et al. PGRN is a key adipokine mediating high fat diet-induced insulin resistance and obesity through IL-6 in adipose tissue. Cell Metab. 2012;15:38–50.
24. Roh E, Song DK, Kim MS. Emerging role of the brain in the homeostatic regulation of energy and glucose metabolism. Exp Mol Med. 2016;48:e216.
25. Jung CH, Kim M-S. Molecular mechanisms of central leptin resistance in obesity. Arch Pharm Res. 2013;36:201–7.
26. Park CB, Lee CH, Cho KW, Shin S, Jang WH, Byeon J, Oh YR, Kim SJ, Park JW, Kang GM et al. Extracellular cleavage of microglia-derived progranulin promotes diet-induced obesity. Diabetes 2024.
27. Lee CH, Song DK, Park CB, Choi J, Kang GM, Shin SH, Kwon I, Park S, Kim S, Kim JY, et al. Primary cilia mediate early life programming of adiposity through lysosomal regulation in the developing mouse hypothalamus. Nat Commun. 2020;11:5772.
28. Song L, Lee C, Schindler C. Deletion of the murine scavenger receptor CD68. J Lipid Res. 2011;52:1542–1550.
29. Tanaka Y, Chambers JK, Matsuwaki T, Yamanouchi K, Nishihara M. Possible involvement of lysosomal dysfunction in pathological changes of the brain in aged progranulin-deficient mice. Acta Neuropathol Commun. 2014;2:78.
30. Napolitano G, Ballabio A. TFEB at a glance. J Cell Sci. 2016;129:2475–81.
31. Terman A, Brunk UT. Lipofuscin: mechanisms of formation and increase with age. Apmis. 1998;106:265–76.
32. Leibiger C, Deisel J, Aufschnaiter A, Ambros S, Tereshchenko M, Verheijen BM, Büttner S, Braun RJ. TDP-43 controls lysosomal pathways thereby determining its own clearance and cytotoxicity. Hum Mol Genet. 2018;27:1593–607.
33. Meneses A, Koga S, O'Leary J, Dickson DW, Bu G, Zhao N. TDP-43 Pathology in Alzheimer's Disease. Mol Neurodegeneration. 2021;16:84.
34. Song Q, Meng B, Xu H, Mao Z. The emerging roles of vacuolar-type ATPase-dependent lysosomal acidification in neurodegenerative diseases. Transl Neurodegener. 2020;9:17.
35. Du H, Zhou X, Feng T, Hu F. Regulation of lysosomal trafficking of progranulin by sortilin and prosaposin. Brain Commun. 2022;4:fcab310.
36. Mauvezin C, Neufeld TP. Bafilomycin A1 disrupts autophagic flux by inhibiting both V-ATPase-dependent acidification and Ca-P60A/SERCA-dependent autophagosome-lysosome fusion. Autophagy. 2015;11:1437–8.
37. Kwon O, Kim KW, Kim MS. Leptin signalling pathways in hypothalamic neurons. Cell Mol Life Sci. 2016;73:1457–77.
38. Frew J, Nygaard HB. Neuropathological and behavioral characterization of aged Grn R493X progranulin-deficient frontotemporal dementia knockin mice. Acta Neuropathol Commun. 2021;9:57.
39. Valdez C, Wong YC, Schwake M, Bu G, Wszolek ZK, Krainc D. Progranulin-mediated deficiency of cathepsin D results in FTD and NCL-like phenotypes in neurons derived from FTD patients. Hum Mol Genet. 2017;26:4861–72.
40. Zhou X, Paushter DH, Feng T, Pardon CM, Mendoza CS, Hu F. Regulation of cathepsin D activity by the FTLD protein progranulin. Acta Neuropathol. 2017;134:151–3.
41. Zhou X, Paushter DH, Pagan MD, Kim D, Nunez Santos M, Lieberman RL, Overkleeft HS, Sun Y, Smolka MB, Hu F. Progranulin deficiency leads to reduced glucocerebrosidase activity. PLoS ONE. 2019;14:e0212382.

42. Jian J, Tian QY, Hettinghouse A, Zhao S, Liu H, Wei J, Grunig G, Zhang W, Setchell KDR, Sun Y, et al. Progranulin recruits HSP70 to beta-glucocerebrosidase and is therapeutic against Gaucher Disease. EBioMedicine. 2016;13:212–24.
43. Valdez C, Ysselstein D, Young TJ, Zheng J, Krainc D. Progranulin mutations result in impaired processing of prosaposin and reduced glucocerebrosidase activity. Hum Mol Genet. 2019;29:716–26.
44. Lee S, Sato Y, Nixon RA. Lysosomal proteolysis inhibition selectively disrupts axonal transport of degradative organelles and causes an Alzheimer's-like axonal dystrophy. J Neurosci 2011;31:7817–30.
45. Boland S, Swarup S, Ambaw YA, Malia PC, Richards RC, Fischer AW, Singh S, Aggarwal G, Spina S, Nana AL, et al. Deficiency of the frontotemporal dementia gene GRN results in gangliosidosis. Nat Commun. 2022;13:5924.
46. Zhou X, Sun L, Bracko O, Choi JW, Jia Y, Nana AL, Brady OA, Hernandez JCC, Nishimura N, Seeley WW, Hu F. Impaired prosaposin lysosomal trafficking in frontotemporal lobar degeneration due to progranulin mutations. Nat Commun. 2017;8:15277.
47. Du H, Zhou X, Feng T, Hu F. Regulation of lysosomal trafficking of progranulin by sortilin and prosaposin. Brain Commun 2022, 4.
48. Zheng Y, Brady OA, Meng PS, Mao Y, Hu F. C-terminus of progranulin interacts with the beta-propeller region of sortilin to regulate progranulin trafficking. PLoS ONE. 2011;6:e21023.
49. Salazar DA, Butler VJ, Argouarch AR, Hsu TY, Mason A, Nakamura A, McCurdy H, Cox D, Ng R, Pan G, et al. The progranulin cleavage products, granulins, exacerbate TDP-43 toxicity and increase TDP-43 levels. J Neurosci. 2015;35:9315–28.
50. Lee CH, Suk K, Yu R, Kim MS. Cellular contributors to Hypothalamic inflammation in obesity. Mol Cells. 2020;43:431–7.

Publisher's note